Physics – Uspekhi **53** (6) 619 – 639 (2010)
© 2010 Uspekhi Fizicheskikh Nauk, Russian Academy of Sciences

CONFERENCES AND SYMPOSIA

PACS numbers: 01.10.Fv, **07.87.+v**, **29.20.–c**, **42.62.–b**, 42.62.Be, 87.50.W-, **87.56.–v**, **87.63.–d**, 95.55.Ev, **96.60.–j**

Nuclear physics, lasers, and medicine (Scientific session of the General Meeting of the Physical Sciences Division of the Russian Academy of Sciences, 14 December 2009)

DOI: 10.3367/UFNe.0180.201006g.0647

The scientific session of the General Meeting of the Physical Sciences Division of the Russian Academy of Sciences (RAS) was held in the Conference Hall of the Lebedev Physical Institute, RAS, on 14 December 2009.

The following reports were put on the session agenda posted on the web site www.gpad.ac.ru of the Physical Sciences Division, RAS:

(1) **Kotov Yu D** (National Research Nuclear University 'Moscow Engineering Physics Institute' (MEPhI), Institute of Astrophysics, Moscow) "High-energy solar flare processes and their investigation onboard Russian satellite missions CORONAS";

(2) **Pakhlov P N** (Russian Federation State Scientific Center 'Alikhanov Institute for Theoretical and Experimental Physics,' Moscow) "Exotic charmonium";

(3) **Shcherbakov I A** (Prokhorov General Physics Institute, RAS, Moscow) "Laser and plasma technologies in medicine";

(4) **Balakin V E** (Center for Physics and Technology, Lebedev Physical Institute, RAS, Protvino, Moscow region) "New-generation equipment and technologies for the ray therapy of oncological diseases using a proton beam";

(5) **Kravchuk L V** (Institute for Nuclear Research, RAS, Moscow) "Development of nuclear physics medicine at the Institute for Nuclear Research, RAS."

Papers based on reports 1, 3, and 5 are published below. The expanded content of the report by Pakhlov is presented in review form in *Physics–Uspekhi* **53** 219 (2010).

PACS numbers: **07.87.+v**, 95.55.Ev, **96.60.–j**
DOI: 10.3367/UFNe.0180.201006h.0647

High-energy solar flare processes and their investigation onboard Russian satellite missions CORONAS

Yu D Kotov

1. Introduction

The Skylab (1973), SMM (Solar Maximum Mission) (1980), Yohkoh (1991), and SOHO (SOlar Heliospheric Observatory) (1995) solar missions created an instrumental revolution in solar studies and opened up the era of solar observations in the UV and X-ray bands with an angular resolution of several arcseconds. Observations from these satellites and from the subsequent TRACE (Transition Region and Coronal Explorer) (1998), CORONAS-F (2001), and RHESSI (Reuven Ramaty High Energy Solar Spectroscopic Imager) (2002) missions have resulted in a new level of understanding of plasma processes in the solar corona [1], thermal and nonthermal processes accompanying the appearance and development of flare structures [2, 3], the dynamics of three-dimensional heliospheric processes, and so on [4]. The impressive progress in digital X-ray optics and spectrometry, which provide huge observational data that give not only rich observational material for professional researchers but also new impressions for the general community, as well as new possibilities to observe the early stages of solar coronal plasma ejections into the interplanetary space, shifted the focus of solar space studies toward precise optical, UV, and X-ray imaging. Such imaging has been performed by the recently launched missions Hinode, (Japan), STEREO (Solar TErrestrial RElations Observatory (NASA), and SDO (Solar Dynamic Observatory (NASA); it is planned to carry out imaging by approved missions Picard (ESA) and Aditay-I (India), and is being discussed as a task for future missions like Solar-C (Japan), Solar Probe (NASA), Solar Orbiter (ESA), and Interhelozond (Russia).

But because the spectrum of solar radiation generated in various electromagnetic and nuclear processes spans 14 orders of magnitude from long-wave radio to high-energy gamma-rays, obtaining adequate data on the energy characteristics and dynamics of physical processes on the Sun requires complex space observations from hard UV to high-energy gamma-ray, as well as the determination of the elemental and isotopic composition of particles ejected by solar flares into the interplanetary space.

Starting from the 1990s, the Russian Academy of Sciences (The Space Council of RAS) and the Russian Space Agency have been carrying out the CORONAS (Russian abbreviation for Complex Orbital Near-Earth Observations of Solar Activity) program by constructing scientific instruments and performing observations from dedicated satellites.

CORONAS-I was the first satellite of this series (March 1994–December 2000). The second was CORONAS-F (July

Yu D Kotov National Research Nuclear University 'Moscow Engineering Physics Institute,' Institute of Astrophysics, Moscow, Russian Federation
E-mail: YDKotov@mephi.ru

Uspekhi Fizicheskikh Nauk **180** (6) 647 – 670 (2010)
DOI: 10.3367/UFNr.0180.201006g.0647
Translated by K A Postnov, E N Ragozin; edited by A M Semikhatov

Uspekhi Fizicheskikh Nauk **180** (6) 647 – 661 (2010)
DOI: 10.3367/UFNr.0180.201006h.0647
Translated by K A Postnov; edited by A M Semikhatov

2001–December 2005). The head scientific institute of these two satellites manufactured in the Yuzhnoe Construction Bureau (CB) (Dnepropetrovsk, Ukraine) was the Pushkov Institute of Terrestrial Magnetism and Radio Wave Propagation (IZMIRAN). On the first of these satellites, after a short period of operation in orbit, the satellite orientation system broke for technical reasons, which made facing the Sun by the instruments and solar panels impossible and stopped the scientific program earlier than was planned. On the second satellite, all on-board systems and scientific instruments smoothly operated during all of its lifetime in orbit. The orbital altitude and inclination were about 550 km and 82.5°.

Scientific instruments onboard CORONAS-F allowed obtaining monochromatic images with high angular resolution, measuring the fluxes and energy spectra of electromagnetic radiation from ultraviolet to gamma-rays, and registering cosmic rays. The main characteristics of the scientific instruments of CORONAS-F are presented in the paper by the CORONAS-F project scientist V D Kuznetsov [5]. Several key specialists who constructed the scientific equipment of this project in 2008 were awarded the Science and Technology Prize of the Government of the Russian Federation "For construction of scientific instruments with new information registration channels of corpuscular and electromagnetic radiation from the Sun, as well as for priority results of observations of solar activity and its impact on Earth obtained by the CORONAS-F satellite."

Book [5] also contains papers with the results of experiments carried out by the CORONAS-F satellite. Most of the observational and telemetric resources were obtained by the SPIRIT instruments constructed at the Lebedev Physical Institute, RAS (LPI). The instruments included the SRT-K solar X-ray telescopes and RES-K X-ray spectrometers. With the latter instrument, the method of multichannel monochromatic imaging spectroscopy of the whole Sun in the X-ray and extreme vacuum UV regions was realized for the first time. The data obtained by these instruments allow measurements of the structure and dynamics of plasma in the upper solar atmosphere in a broad range of parameters: from the chromosphere to five solar radii in altitude, from 10^3 to 5×10^6 K in temperature, from several seconds to several solar rotational periods in the duration of observations, with an angular resolution of 3–5 arcsec. The data obtained were used to construct modified models of energy release in flares, which effectively work under low-density coronal plasma conditions and are in agreement with experimental results [6].

An important advantage of the scientific instruments of the CORONAS-F satellite is the ability to conduct complex studies of electromagnetic and corpuscular radiation from active solar processes in the rangle from vacuum UV to high-energy gamma rays. The maximum energy of gamma-ray photons registered from solar flares was 300 MeV [7, 8]. A comparison of the registration time of gamma rays from $\pi^0 \to \gamma + \gamma$ decays and energetic solar neutrons produced by accelerated protons (nuclei) in the solar atmosphere with the characteristic times of soft gamma-ray emission and gamma-ray emission lines led to the conclusion that the acceleration of protons to energies ~ 1 GeV occurred in the flare region. A comparison of these emissions with the time of arrival of high-energy protons from these flares on Earth suggested that in at least three powerful flares of classes X17.2, X28.0, and X7.0, protons left the solar atmosphere immediately after having been accelerated. The authors of [8] concluded that models of particle acceleration that are consistent with experimental data at lower energies cannot explain the experimental data in the most energetic part of the spectrum of neutral radiation from flares.

2. The CORONAS-PHOTON satellite

The CORONAS-PHOTON satellite is the third in the solar program. The head scientific institute for this project is the National Research Nuclear University 'Moscow Engineering Physics Institute' (MEPhI). The satellite was manufactured at the Science and Research Institute of Electromechanics (NIIEM) (Istra, Moscow region). The satellite, with the weight of 1860 kg, including 600 kg of scientific payload, was launched on 30 January 2009 into an orbit with the altitude about 565 km and inclination 82.5°. The daily traffic of the scientific information transmitted is not less than 1 Gb.

The satellite was initially scheduled for launch at the beginning of the 24th solar cycle using the prediction by NASA specialists (USA) in 2006. The forecast of solar activity in the 24th cycle calculated by the NASA experts in 2006 and 2009 is shown in Figs 1a and 1b [9, 10]. The broken line shows the actual monthly averaged solar activity. But until the end of 2009, the solar activity was very low, and the experts had to correct their predictions by shifting the maximum activity from the middle of 2010 to the middle of 2013, i.e., by three years! This time lag and the simultaneous decrease in the activity intensity at the maximum by almost two times (!) show how uncertain the current methods of solar activity forecast are.

The anomalously long decay phase of solar activity observed in the 23rd cycle gave rise to assumptions about the forthcoming Maunder minimum. At least, the decay of the 23rd cycle up to the end of the 23rd cycle is similar to that of the 4th cycle. The 5th cycle showed a very low activity at the maximum, which apparently resulted in climate cooling in the 1800s due to a slight decrease in solar radiation. At the same time, unexpectedly, numerous strong solar flares were

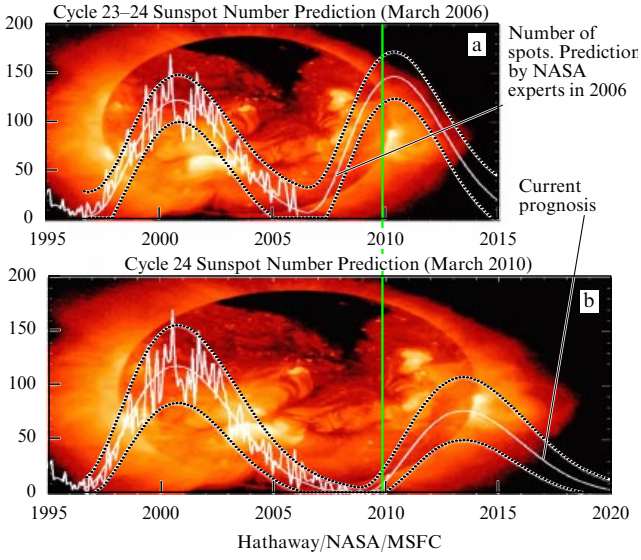

Figure 1. Solar activity in the 23rd and 24th cycles. (a) Prognosis made in 2006 and (b) the current (corrected) prognosis. The vertical line indicates the current date. The broken line shows the measured monthly number of solar spots. The solid line shows the prognosis of solar activity, and the dashed line indicates the prognosis uncertainty.

Table 1. Data on three flares [22].

Characteristic	3 June 1982	24 May 1990	4 June 1991
Attenuation constant of the γ-line 2.2 MeV, s	160 ± 30	47 ± 04 190 ± 30	420 ± 50 1600 ± 400
Attenuation constant of γ-lines 4–7 MeV, s	70 ± 5	28 ± 04 230 ± 30	300 ± 100
Attenuation constant of γ-photons from π^0-decay τ_1 (fast component), s	68 ± 8	30 ± 5	720 ± 360
Attenuation constant of γ-photons from π^0-decay τ_2 (slow component), s	700 ± 180	> 1000	3000 ± 200
Duration of generation of neutrons with the energy above 100 MeV, s	> 300	1130	~ 4000
Neutron luminosity $T > 100$ MeV, sr^{-1}	8×10^{28}	$(3.8 \pm 0.3) \times 10^{30}$	$\sim 1 \times 10^{29}$

detected at the decline of the 23rd cycle. Numerous observational data on the extremely powerful solar flares in October–November 2003 are systematically presented in papers [11, 12].

Therefore, there are grounds to expect that the 24th cycle will be notably different from many previous ones, and hence the detailed study of solar radiation in the current cycle can give the opportunity to better understand the role of solar–terrestrial relations in the emerging tendency of global warming.

The usefulness of observational data on gamma-ray emission from several MeV up to 300 MeV, which was detected in the extreme solar flare on 29 January 2005, is demonstrated in paper [13]. Comparison of these data with the light curve below 2.2 MeV showed that both protons with energies up to 10 MeV and electrons were accelerated during the main phase of the flare in the magnetic field of the active region. The light curve at energies $E > 60$ MeV is similar to that at lower energies, although some fraction of the emission can be produced by the long-lived component of high-energy photons. The background and statistical limitations prevent using the experimental data to quantitatively determine the delayed radiation and its intensity.

The characteristics of high-energy emission from the extreme flare studied in [13] do not fully correspond to the observations of the high-energy radiating flares in 1991 by SMM [14, 15], CGRO (Compton Gamma Ray Observatory) [16], Gamma-1 [17–19], and Granat [20, 21]. As an example, Table 1 from paper [22] shows the data on three flares, including light curves in nuclear lines, high-energy emission, and high-energy neutrons that reached Earth nondecayed.

It turned out that the high-energy emission contains two time components, with one having the duration of a few hours. From the spectral shape, we can conclude that the high-energy radiation was generated in π^0-meson decays. Because low-energy channels do not reveal variations on this time scale, it is necessary to assume either a long retention of high-energy protons (nuclei) in some magnetic traps with a high density sufficient for meson production, or the existence of a specific acceleration mechanism of high-energy protons without visual manifestations of the injection process and the initial acceleration. The obtained observational data led to the following conclusions.

• Solar neutrons with energies $E > 200$ MeV are produced during a time period lasting more than 10–60 min.

• The duration of the formation of high-energy neutrons is comparable to that of γ-quanta and pions.

• The light curve of the 2.2 MeV line does not reflect the duration of generation of high-energy solar neutrons, although it is probably consistent with the formation of solar neutrons with energies 1–100 MeV.

The events of 4 and 6 June were registered in Japan by a neutron monitor (64 m^2) and neutron and muon telescopes.

The high-energy emission observed by the Gamma-1 satellite led to the conclusion that

• in the active stage, there are short outbursts lasting less than 0.2 s;

• electrons and ions are accelerated simultaneously, their flux ratio being 100–1000;

• electrons are distributed isotropically by angle, while protons are collimated.

We also note the problem of 'electron-dominated' flares, in which the flux ratio in nuclear lines to the bremsstrahlung radiation of electrons is 10 times smaller than in 'standard' flares. It is necessary to experimentally confirm and explain the following features of such flares:

• a flat spectrum (with the spectral index $\delta \sim 2$) at energies around 1 MeV;

• a small contribution from nuclear lines;

• a high degree of 'pulsingness' similar to cosmic gamma-ray bursts;

• the independence of the spectral index from the heliocentric angle, suggesting a low degree of anisotropy of the emitting particles.

Therefore, due to the paucity of observational data on high-energy radiation from solar flares obtained so far, the long-term acceleration/retention of high-energy protons (and, possibly, electrons) remains a puzzling issue in the physics of solar flares.

We note that since the early 1990s, high-energy gamma-ray radiation has not been registered, mainly due to the lack of relevant instruments aboard solar missions launched in the last 15 years (with the exception of the CORONAS satellites). Nuclear emission with energies up to 10 MeV with high energy resolution in lines could be detected by the RHESSI satellite, but the efficiency of its germanium detector substantially decreases in the range above 1 MeV.

The parameters of instruments are determined by the spectral shape of emission generated in a flare by thermal and nonthermal mechanisms in the loop, as shown schematically in Fig. 2 [24]. The initial energy release due to a change in the magnetic field configuration (magnetic field

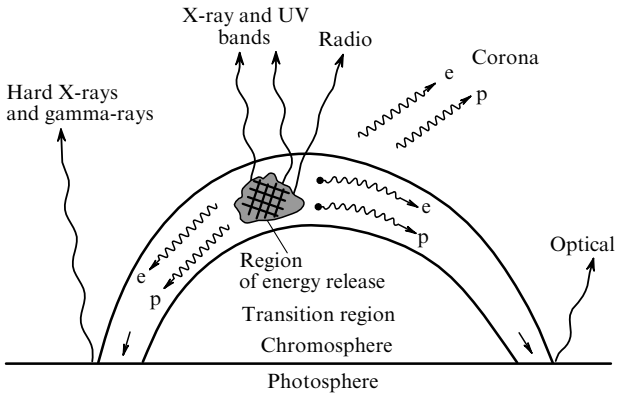

Figure 2. The structure of a magnetic arch.

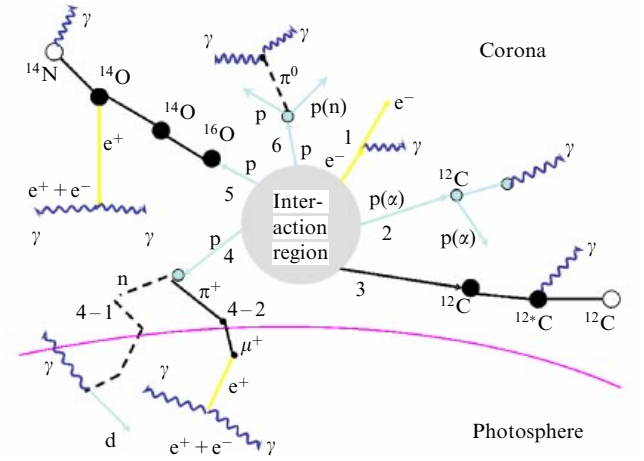

Figure 3. High-energy processes of interaction of accelerated particles in the solar atmosphere resulting in gamma-ray emission and neutrons observed near Earth.

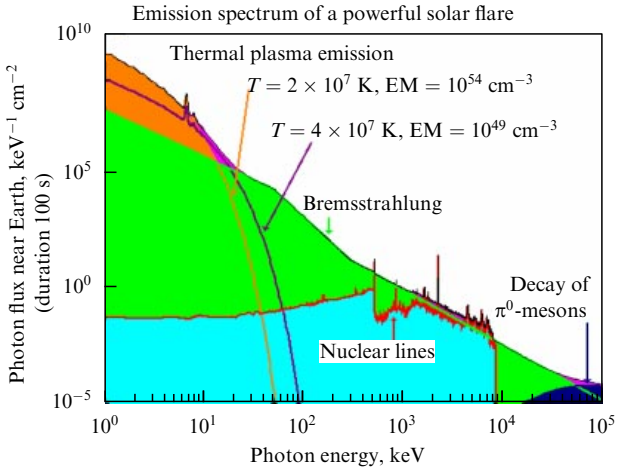

Figure 4. The composite emission spectrum of a typical strong flare registered near Earth over 100 s. EM is the emission measure.

line reconnection) heats up the coronal plasma and leads to simultaneous (or sequential) acceleration of electrons, protons, and nuclei. At the looptop, where the density is small and the temperature reaches 15–20 mln K, thermal hard UV and soft X-ray emission is generated, and the current of charged particles generates radio emission at different frequencies.

The density at the tip of the loop is usually not sufficiently high to effectively produce bremsstrahlung emission of electrons and nuclear emission from the interaction of accelerated protons and nuclei, and therefore the radiation from these particles is observed after they reach the chromosphere. In the simplest loop model, protons (nuclei) and electrons move along quasispiral trajectories toward the footpoints. For a dipole magnetic field, an oscillating motion of particles between loop feet can occur, which leads to quasiperiodic oscillations (QPOs) of radio and hard X-ray emission. The period of such oscillations is determined by the size of the loop, its magnetic field parameters, and the energy spectrum of captured particles. The actual picture of the process can also be determined by the variability of particle injection into the loop and excitation of wave processes there. QPOs during solar flares have been observed many times in different electromagnetic bands from radio to gamma rays [25–27]. The observed periods are in the range from several milliseconds (in the radio emission) to several hundred seconds (in the hard emission).

The results of observations of the solar flare of 10 June 1990 by the Granat observatory are reported in [28]. The duration of the flare in the 8–20 keV range was 2 h, and the X-ray pulsation period was 143.2 ± 0.8 s. The maximum pulsation amplitude was 5% of the total intensity. Hence, for example, the size of the magnetic loop was $(1-3) \times 10^{10}$ cm.

A model of quasiperiodic pulsation generation was discussed in [2, 29]. The measured parameters of Alfvén oscillations allow estimating the temperature and density of plasma evaporating from the loop feet [30].

In the flare of 1 January 2005, 2–6 MeV, 40 s quasiperiodic pulsations were registered by the SONG (SOlar Neutrons and Gamma-quanta) device aboard the CORONAS-F satellite [31]. These QPOs were confirmed by observations of this flare by the Nobeyama radioheliograph and RHESSI in the 80–225 keV range.

Clearly, obtaining statistically reliable data over periods down to several milliseconds in the hard X-ray and gamma-ray range requires instruments with a large effective area, high signal-to-noise ratio, and high performance channels of data transmission to Earth.

When accelerated (nonthermal) electrons and nuclei enter dense chromospheric layers, different interactions occur, as shown schematically in Fig. 3. The electromagnetic and nuclear interactions result in the total spectrum shown in Fig. 4 [32]. The intensity and energy spectrum of individual radiation components provide information on the composition and energy of the accelerated particles, their acceleration rate, the composition of the accelerated medium, and other characteristics of the acceleration process [33–37]. The major part of the energy of accelerated electrons and protons with energies up to several tens of MeV is lost in the atmosphere due to Coulomb losses, which heat up and evaporate the matter along magnetic field lines.

Accelerated electrons (line 1 in Fig. 3) emit bremsstrahlung radiation and form a featureless continuum spectrum with the maximum energy of the order of the initial kinetic energy of electrons. At subrelativistic and relativistic energies of electrons, photons are emitted mostly in the forward direction within the characteristic angle $\theta \sim 1/\gamma$, where γ is the particle Lorentz factor. For a narrow beam of electrons

with different energies, the observed photon spectrum depends on the angle between the beam direction and the line of sight. This feature can be used for statistical analysis of a sample of flares to estimate the angular distribution of emitting electrons. The dependence of the spectral characteristics of X-ray emission from solar flares on the angular anisotropy of accelerated particles was studied in [37] for 10–600 keV X-ray emission and different distributions of the accelerated electrons. A comparison of the experimental data obtained by the SIGNE-2MZ detector onboard Venera-13 and 14 spacecraft with the results of calculations in [37] suggests [38] that the discovered spectral softening toward the center of the solar disk is most likely due to an angular anisotropy of the accelerated electrons. There are indications that the angular distribution of electrons changes in different flares.

The angular anisotropy of interacting electrons can lead to linear polarization of the observed X-ray and gamma-ray emission. The possibility to study the angular distribution of accelerated particles from polarization data was first suggested in [39]. First polarization measurements of X-ray emission from solar flares were carried out by LPI researchers using satellites of the Interkosmos series [40]. The polarization values measured for several flares are consistent with the models in [41, 42] and, despite large measurement errors, suggest a strong angular anisotropy of fast electrons. We note that the originally reported value of the mean polarization in three weak flares in October–November 1970 was $40 \pm 20\%$ [43], but it was later decreased to 20%. In the Interkosmos-11 experiment, the polarization measured in two flares at energies about 15 keV was a few percent.

In the 1990s, no polarization measurements were performed from satellites. They were renewed in the early 2000s from the satellites CORONAS-F (SPR-N polarimeter) and RHESSI [46]. Although the instruments aboard RHESSI were not originally designed for polarization studies, it turned out that such measurements could be made by the corresponding selection of events in two-section detectors. In the 0.2–1 MeV emission observed from two flares, the degree of linear polarization was 0.21 ± 0.09 (23.07.2002) and -0.11 ± 0.05 (28.10. 2003) [47].

During four years of operation, 128 solar flares were detected by the SPR-N polarimeter, of which 25 were sufficiently bright to search for the azimuthal scattering asymmetry due to linear polarization. In the flare of 29 October 2003, the degree of polarization was measured to be more than 70% in the 40–60 keV and 60–100 keV channels and around 50% in the 20–40 keV channel [45]. Because the flare was close to the center of the solar disk (S15W02), these values cannot be made consistent with theoretical estimates obtained under the assumption that the loop has no anomalously high inclination to the solar surface. For other flares, only the upper limits of the fraction of polarized emission were obtained in the range from 8% to 40%.

These polarization measurements show an insufficient sensitivity of the instruments used and a significant contribution from background effects, because the method of Compton scattering allows an azimuthal asymmetry of 10–20%.

During nuclear interactions, the accelerated protons, α-particles, and ^{3}He nuclei (line 2 in Fig. 3) can excite the nuclei of the medium, which emit gamma-ray lines when transiting to the ground state. Due to the relatively small Coulomb repulsion, the threshold energy for proton excitations is close to the energy of gamma-ray photons. The excitation cross section is maximal at energies of several tens of MeV, and hence the effects of line broadening due to the nuclear recoil are small for mean and heavy nuclei of the medium. The most intensive lines are in the range from 0.847 MeV for ^{56}Fe to 6.13 MeV for ^{16}O. Using the line intensity ratio, we can determine the number density ratio of elements in the solar atmosphere in the region of stopping of the accelerated protons and α-particles. Using the intensity ratio of lines with a different excitation threshold, the energy spectrum of interacting protons can be estimated. This estimate can be done in the energy range from several MeV to several tens of MeV.

Measurements of the intensities of 0.429 MeV and 0.478 MeV lines of the rare nuclei ^{7}Be and ^{7}Li that are formed in $\alpha-\alpha$ interactions during the flare have important astrophysical applications. Due to the equal masses of the nuclei colliding in this reaction, the Doppler broadening of the emerging line is significant (see the detailed description of the possibilities of the nuclear spectroscopy of solar flares in [48, 49]).

When accelerated nuclei are excited (line 3 in Fig. 3), the emerging radiation is transformed due to the motion of the nuclei (line shift and broadening). Separating these lines from the continuum, it is possible to determine the fraction of the accelerated nuclei as a function of the ionization potential of the atom.

High-energy protons ($T > 300$ MeV) can produce neutral (line 6) or charged (line 4) pions, which subsequently decay (see Fig. 3). Positrons formed in such decays are stopped in the medium (the stopping time scale is determined by the medium density) and annihilate with electrons to produce a 0.5 MeV line. Gamma-photons from $\pi^0 \rightarrow \gamma + \gamma$ decays form a broad continuum with a maximum at 70 MeV for the isotropic distribution of accelerated protons. When π^0 are produced by a narrow beam of protons, the maximum of the emerging gamma-ray spectrum is shifted depending on the angle between the beam direction and the line of sight. In principle, when the statistics of high-energy photons are sufficiently high, it is possible to distinguish pion generation produced by a beam or isotropic particle distribution.

Finally, the interaction of energetic protons and nuclei with a medium can produce neutrons with energies from a few MeV to several hundred MeV and higher, depending on the energy of interacting particles. Low-energy neutrons slow down in the photosphere and can be captured by protons in the reaction $n + p \rightarrow d + \gamma$ ($E_\gamma = 2.2$ MeV). A significant fraction of high-energy neutrons can be injected into the interplanetary space, and some of them can reach Earth. High-energy neutrons with energies above 200 MeV and gamma-quanta from $\pi^0 \rightarrow 2\gamma$ decays are produced by one population of interacting hadrons with similar (nuclear) cross sections, and therefore time profiles of their intensities must be similar. In particular, for the power-law energy spectrum $dN(T)/dT \sim T^{-3}$, the maximum production efficiency of these particles occurs at proton energies about 700 MeV.

Therefore, the goal of instruments in the CORONAS-PHOTON project is to obtain observational data, in particular, in order to clarify the questions of the generation and development of high-energy processes on the Sun. The principal advantage of studies from CORONAS-F and CORONAS-PHOTON satellites in comparison with satellite experiments of the 1990s is the possibility to register, in addition to gamma-ray emission, flare processes in the hard UV and X-ray bands with a high angular resolution of several

arcseconds, using instruments on the same satellite or on other solar satellites currently in orbit.

3. Goals of the CORONAS-PHOTON project

The following goals of the CORONAS-PHOTON project have been established.

• To carry out detailed observations of processes leading to the appearance of solar flares, to determine their periodicity and intensity, and to improve models of short-term and long-term forecast of solar activity.

• To obtain information on the type, energy, and time behavior of emissions generated in flares and to update models of acceleration of particles (electrons, protons, and ions) up to ultrarelativistic energies, of their propagation in the solar atmosphere, and of the ejection of plasma and energetic particles into the interplanetary space.

• To observe coronal mass ejections and eruptive prominences and to determine the physical state of plasma in these processes: its temperature, electron and ion density, and the differential emission measure. Measurements of the physical state of plasma are needed to calculate the energy balance of active coronal processes.

• To obtain time-averaged systematic data with high absolute precision on solar radiation from the UV range to high-energy gamma rays.

• To determine characteristics of the particle acceleration process using data on high-energy radiation from flares.

• To determine the amount of accelerated nuclei and electrons and their energy spectrum, including particles with the highest energy.

• To determine the acceleration rate, dynamics, and propagation of particles (time characteristics and pulsations).

• To study the dynamics of propagation of particles in the solar atmosphere and their escape into the circumsolar space (thin or thick target of interaction and angular resolution).

• To obtain data on the medium composition where particle interaction occurs.

• To determine the composition of accelerated particles, which is different from the composition of the surrounding medium due to selection effects of the acceleration mechanism.

• To establish the similarity (or difference) between the acceleration of protons (nuclei) and that of electrons.

• To determine the relation between the particle acceleration and heating mechanisms.

• To study the nature of electron-dominated flares.

• To investigate the formation of rare elements from the interaction of protons and light nuclei in flares.

The TESIS (TElescope Solar/Imaging Spectrometer) telescope has a unique sample of imaging channels. In addition to simultaneously obtaining data with other CORONAS-PHOTON instruments, this telescope has its own program to study the dynamics of long-lived plasma structures in the solar corona, such as active regions and coronal holes.

***Additional scientific goals of the CORONAS-PHOTON project include*:**

• Astrophysics:

— studies of X-ray and gamma-ray radiation from cosmic gamma-ray bursts.

• Cosmic-ray physics:

— measurement of characteristics and the pitch–angle distribution of cosmic rays (electrons, protons, and alpha-particles) along the satellite orbit.

• The physics of Earth's atmosphere:

— monitoring of upper Earth's atmosphere from the absorption of hard X-ray radiation from the Sun;

— studies of characteristics of ultra-short gamma-ray flares formed in the upper Earth atmosphere.

The project participants who designed and manufactured the scientific payload of the experiment are mostly Russian researchers from different scientific and industrial bodies: Yu D Kotov, V N Yurov, A I Arkhangelsky, M V Bessonov, A S Buslov, K F Vlasik, A S Glyanenko, V V Kadilin, P A Kalmykov, A V Kochemasov, Ye E Lupar', I V Rubtsov, Yu A Trofimov, V G Tyshkevich (MEPhI, the head scientific institute of the CORONAS-PHOTON project); R S Salikhov, Yu I Alikin, M P Gassieva (NIIEM); S I Boldyrev, V D Kuznetsov, N I Lebedev (IZMIRAN); S A Bogachev, Yu S Ivanov, A P Ignatiev, S V Kuzin, A A Pertsov (LPI); R L Aptekar, S V Golenetsky, V A Dergachev, V N Iljinsky, E M Kruglov, V P Lazutkov, G A Matveev, E P Mazets, M I Savchenko, D V Skorodumov, A V Ulanov, M V Ulanov, D D Frederiks, Yu A Chichikalyuk [Ioffe Physics Technical Institute (PTI), RAS]; K V Anufreichik, M V Buntov, I V Kozlov, A V Nikoforov, A D Ryabova, I V Chulkov [Space Research Institute (IKI), RAS]; Yu Yu Denisov, V V Kalegaev, M I Panasyuk [Skobeltsyn Nuclear Physics Research Institute of the Lomonosov Moscow State University (NIIYaF, MSU)], as well as specialists from Ukraine: A V Dudnik, I I Zalyubovsky, B K Persikov [Karazin Kharkov National University (KNU)]; India: A Nandi, S Srikumar, S K Chakrabarty (Indian Center for Space Physics, Kolkata), A R Rao [Tata Institute of Fundamental Researches (TIFR), Mumbai], S Sankaratil (Vikram Sarabhai Space Center, Thiruvanthapuram), and Poland: J Silvestr [Space Research Center of the Polish Academy of Sciences (SRC PAS), Wroclaw].

The scientific payload of the CORONAS-PHOTON satellite includes:

• Eight instruments designed for registering electromagnetic radiation from the Sun in a wide range of spectra from near-electromagnetic waves to gamma radiation, as well as solar neutrons: N-2M, Konus, Pinguin, BRM (Rapid X-ray Monitor), RT-2, SphinX, PHOKA, SOKOL (Solar Oscillations);

• TESIS telescope, which has several individual channels;

• two instruments to detect charged particles (protons, electrons, and nuclei): STEP-F and Electron-M-Peska;

• a magnetometer (SM-8M) to measure Earth's magnetic field in the satellite orbit;

• two service systems (the BUS-FM control block and SSRNI science data collection and registration system).

Radiation registered by different instruments and institutes where the instruments were designed are listed in Table 2. Payload location on the satellite is shown in Fig. 5. The longitudinal axis of the satellite on the day part of the orbit is oriented to the solar disk center with an accuracy of ± 2 arcminutes, the rate of destabilization of the longitudinal axis is less than $7.2'' \text{ s}^{-1}$, the time of the orientation recovery after coming out of the shadow is about 80 s, and the timing accuracy is better than 1 ms relative to Coordinated Universal Time.

The collection of telemetry data and its storage and transmission is shown schematically in Fig. 6. As seen from this scheme, obtaining and diffusing information was coordinated by MEPhI. The satellite control and handling were also done there. Information resources allowed simulta-

Table 2

Instrument	Main characteristics. Registration band	Designer institute
Natalya-2M high-energy radiation spectrometer	Gamma rays (0.3–2000 MeV), amplitude and time spectra Neutrons (20–300 MeV)	MEPhI, Moscow
RT-2 low-energy gamma-ray telescope spectrometer	X-rays (100–150 keV) in phoswich mode Gamma rays (0.10–2 MeV) in spectrometer mode	TIFR, Mumbai, India
Pinguin-M hard X-ray polarimeter spectrometer	X-rays (20–150 keV), linear polarization measurement X-rays/gamma rays (0.015–5 MeV) X-rays (2–10 keV)	PTI, RAS, St. Petersburg
TESIS solar telescope spectrometer SphinX block (in TESIS)	Telescope in the MgXII (8.42 Å) line Spectroheliometer (280–330 Å) Telescopes (130–136 Å and 290–320 Å) Coronograph (29–32 nm), corona images up to four solar radii Soft X-ray spectrum (0.5–15 keV)	LPI, RAS, Moscow CSR PAS, Wroclaw, Poland
BRM (Rapid X-ray Monitor)	X-rays (20–600 keV), six channels	MEPhI, Moscow
PHOKA Solar hard UV-radiation monitor	Soft X-rays (1–11 nm) Hard UV radiation (27–37 nm) Hard UV radiation in the hydrogen line 121.6 nm	MEPhI, Moscow
Konus-RF X-ray and gamma spectrometer	Spectra in the X-ray and gamma-ray bands (10 keV–12 MeV)	PTI RAS, St. Petersburg
SOKOL multichannel photometer	Measurement of small periodic variations of solar radiation at wavelengths 280, 350, 500, 650, 850, 1100, 1500 nm	IZMIRAN, Troitsk, Moscow region
Electron-M charge particle analyzer	Protons (1–20 MeV) Electrons (0.2–2 MeV) Nuclei ($Z < 26$), 2–50 MeV per nucleon	NIIYaF, MSU, Moscow
STEP-F satellite telescope of electrons and protons	Protons (9.8–61 MeV) Electrons (0.4–14.3 MeV) Alpha-particles (37–246 MeV)	KNU, Kharkiv, Ukraine
SM-8M magnetometer	Measurement of three components of terrestrial magnetic field ($-55 - +55$ μT)	NPP Geologorazvedka, St. Petersburg
Data collection and registration system (SSRNI)	Collection of scientific information, issuing digital commands for scientific payload. Storage device capacity 1 Gbyte	IKI, RAS, Moscow
BUS-FM control and connection block	Power supply and generation of commands for scientific payload	IKI, RAS, Moscow

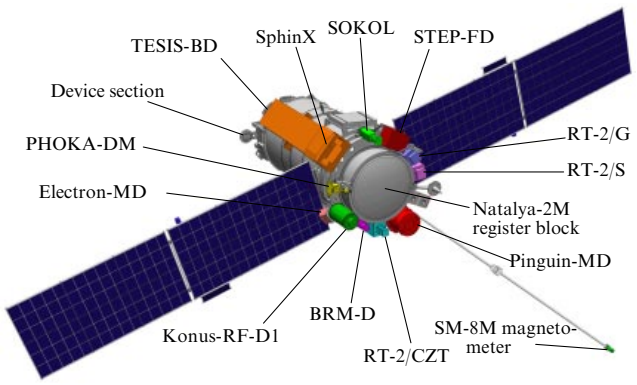

Figure 5. Location of the scientific instruments on the CORONAS-PHOTON satellite, oriented to the center of the solar disk.

neous operation of all instruments. A detailed description of the devices, their testing at different prelaunch stages, as well as the organization and functioning of the Express Data Analysis and Storage Center are presented in [50–53].

4. Preliminary data obtained from February to December 2009

As noted in Section 2, the beginning of the new solar activity cycle was delayed by about three years; during this period, the Sun was in an extremely quiet phase with almost no flares. During the operation time, the Pinguin-M soft X-ray detector with the low energy threshold 2 keV registered 172 solar flares, including 101 class-B flares and 13 class-C flares. Many class-A and weaker flares were detected by the SphinX instrument (1.5–15 keV).

The discrepancy of the CORONAS-PHOTON data with the GOES data is due to the former having orbital cycles where the satellite enters the shadow, the lack of data transmission from the satellite for technical reasons during relatively short intervals, and the variable background produced by particles of the inner and outer radiation belts of Earth. In different detectors, depending on their thickness, size, and other parameters, the background plays a significantly different role. In particular, in optical to soft X-rays, the thickness and size of the detector is small, and its role is therefore insignificant. On the other hand, in hard X-rays and especially gamma-rays, the detector parameters are important. For example, Fig. 7 shows the instrumental noise in Natalya-2M detectors depending on the orbital location of the satellite.

During the discussed unique quiet period of solar activity, it was possible to study the simplest, 'elementary' dynamical processes in the solar corona in the simplest magnetic field configurations.

During this period, the TESIS experiment aboard the CORONAS-PHOTON satellite obtained the following results:

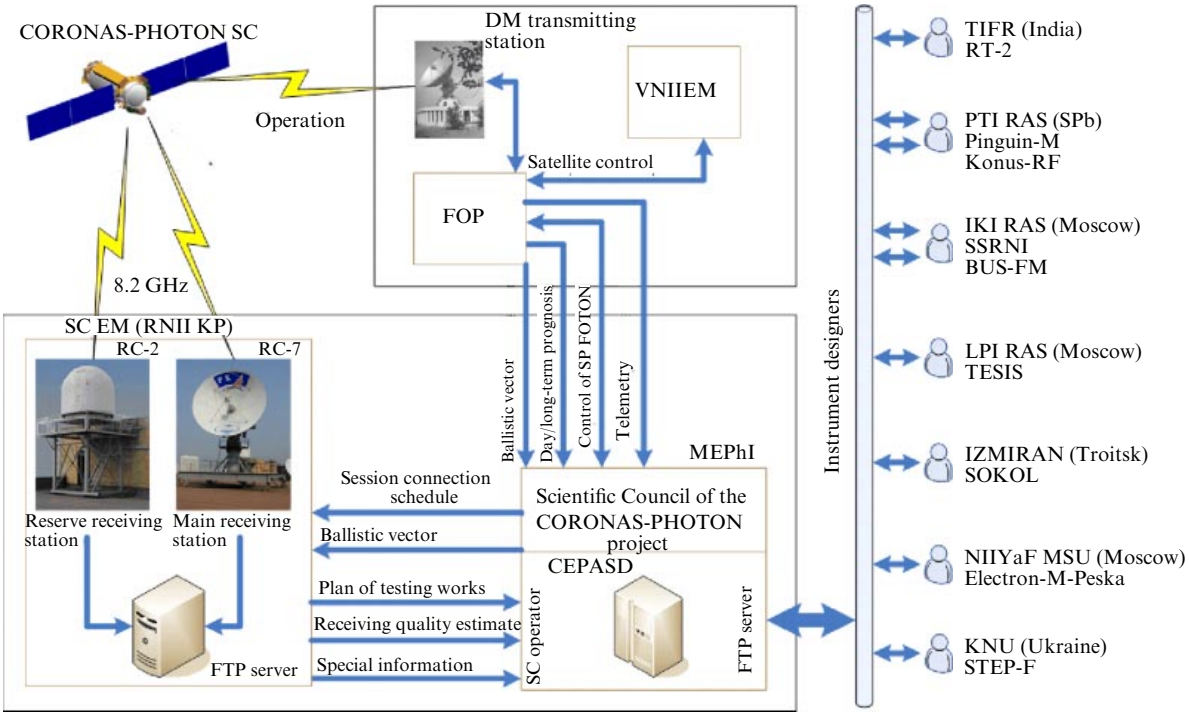

Figure 6. The structure of the ground-based complex of collection, storage, express analysis, and diffusion of telemetry of scientific data and the organization of the scientific operation. VNIIEM — Research and Production Firm 'Iosifyan All-Russian Science and Research Institute of Electromechanics' (Moscow), FOC — Flight Operation Center, SP — Scientific Payload, DM — Defense Ministry, SC EM — Science Center of Earth Monitoring, RNII KP — Russian Science and Research Institute of Space Device Manufacturing, RC-2 and RC-7 — receiving facilities, FTP — file transfer protocol, CEPASD — Center for Express Processing, Accumulation, and Storage of Data of the Institute of Astrophysics, MEPhI.

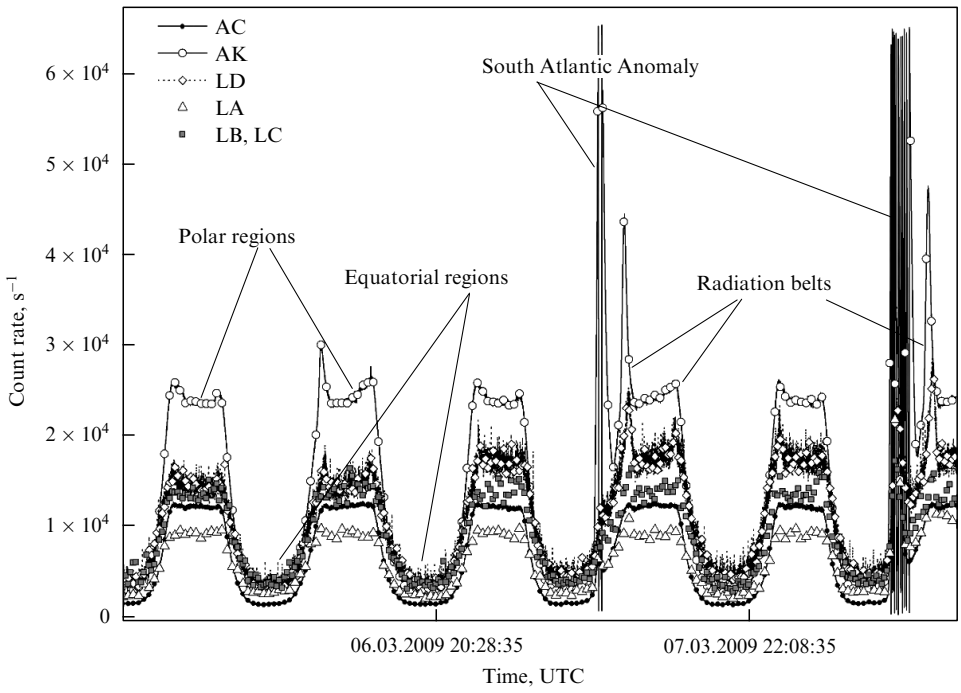

Figure 7. Background light curve of detectors AC, AK, LD, LA, LB, and LC of the Natalya-2M instrument related to the latitude dependence of proton and electron fluxes in the inner and outer radiation belts of Earth.

• for the first time, short-wavelength images of the solar corona at distances from 0.5 to 1.5 solar radii were obtained;

• jointly with the Hinode Observatory (Japan), a new type of 'hot' coronal mass ejection with the plasma temperature 1×10^6 K was discovered;

• for the first time, the process of 'detachment' of the coronal mass from the solar magnetic field was registered in detail;

• for the first time, the dynamics of hot coronal X-ray points and chromospheric spicules were measured with the

Table 3. Parameters of measurement channels.

Channel	Filter (nominal thickness, nm)	Visible light background suppression (contribution of the residual background to the signal)	Band, nm	Note
Main channels				
No. 1 (Visible light)	Glass KS-4B	—	155 – 1100	Technological optical channel
No. 3 (Ly-α)	Interference filters	3×10^8 (21%)	116 – 125	Lyman-α measurement channel
No. 6 (Cr/Al)	Cr/Al (100/200)	10^8 (35%)	(0.5 – 7) and (27 – 37)	Photodiode evaporated filter
No. 7 (Ti/Pd)	Ti/Pd (200/100)	5×10^7 (52%)	0.5 – 11	Photodiode evaporated filter
Calibration channels				
No. 2 (Ly-α calibration)	Interference filters	3×10^8 (25%)	116 – 125	Lyman-α measurement channel
No. 5 (Cr/Al calibration)	Cr/Al (100/200)	3×10^7 (65%)	(0.5 – 0.7) and (27 – 37)	Photodiode evaporated filter
No. 4 (Ti/Pd calibration)	Ti/Pd (200/100)	10^7 (86%)	0.5 – 11	Photodiode evaporated filter

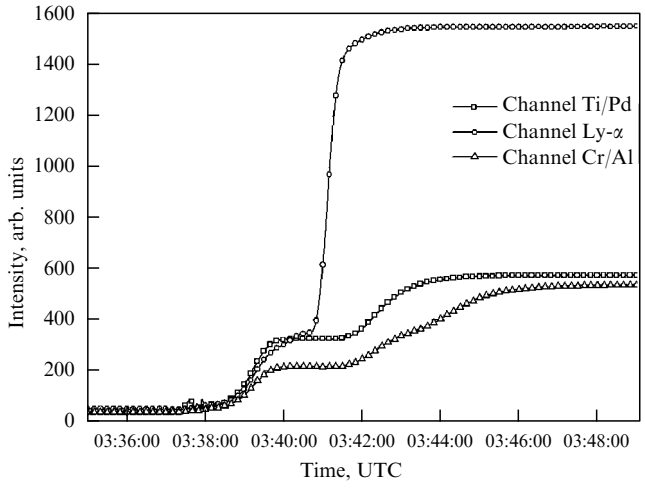

Figure 8. Light curve of the vacuum UV radiation registered by the PHOKA detector during the satellite emergence from the Earth shadow in the period of quiet Sun.

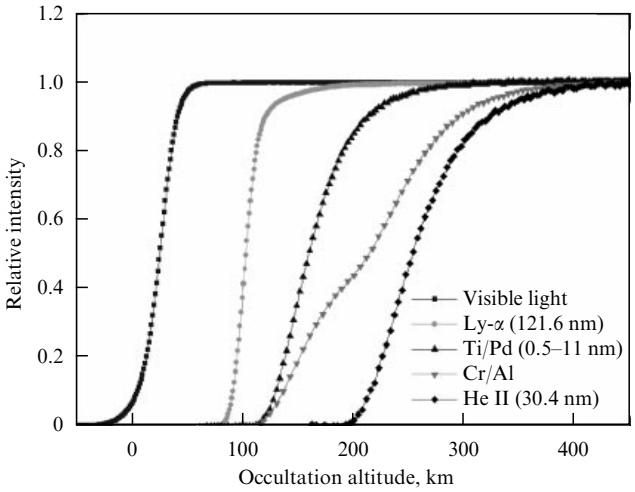

Figure 9. The relative vacuum UV fluxes as a function of the occultation altitude (minimal altitude above Earth of the line of sight from the detector to the Sun).

time resolution about 1 s. The best previous measurements obtained by SOHO (ESA) had the accuracy about 60 s;

• for the first time, a new type of event, flares of solar radiation in bright coronal points and active regions lasting less than 1 min, was discovered. Previously, such rapid solar activity was unknown due to the impossibility of solar imaging with an angular resolution better than 1′.

• for the first time, precise measurements of temperature in hot ($T > 5 \times 10^6$ K) microstructures of the solar corona were performed by spectroscopic methods. The characteristic distributions of the instant and mean temperatures over an ensemble of structures were found.

Solar images obtained by the TESIS telescope are publicly available from the site www.tesis.lebedev.ru of the solar X-ray astronomy laboratory, LPI [54].

The continuous monitoring of the vacuum UV radiation flux was performed every 0.4 s by the PHOKA radiometer aboard the CORONAS-PHOTON satellite in the 0.5–11 nm, 27–37 nm, and 116–125 nm bands. A new type of photodiodes, AXUV-50 (Absolute eXtreme UV), was used. The parameters of the spectral channels and light filters used are presented in Table 3. The calibration filters open only during calibration intervals. The results of occultation measurements (for the satellite), shown in Fig. 8 for the satellite coming out of the Earth shadow, allows estimating the visual light contribution to the measured fluxes and measuring the absorption properties of the upper atmosphere of Earth each time the satellite enters and emerges from the shadow.

The recalculated flux attenuation as a function of the occultation altitude (the minimum altitude of the see-through region of the atmosphere) is shown in Fig. 9.

The 0.5–7 nm flux measured by the PHOKA radiometer on 28.02.2009 is 6.0×10^{-5} W m^{-2}.

When calculating the absolute flux from observational data, the detailed spectral shape should be known. The above flux was obtained using the reference solar spectrum recommended by LASP (Laboratory for Atmospheric and Space Physics, USA) for the period of low solar activity and absence of flares. On the same date, the XPS (X-ray Polarization Spectrometer) of LASP aboard the American satellite SORCE (SOlar Radiation and Climate Experiment) measured the flux 7.1×10^{-5} W m^{-2} in the same band (with methodical errors of 12–30%) [55].

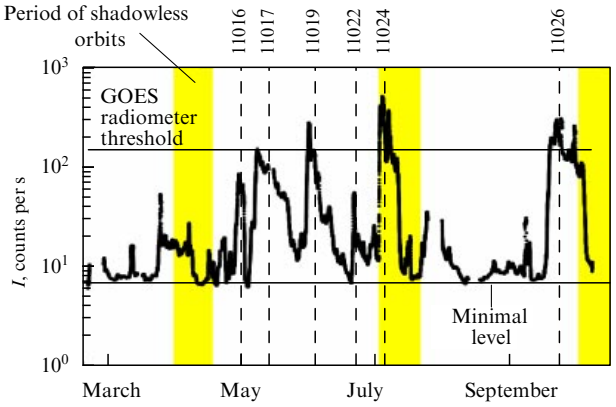

Figure 10. Example of the keV light curve in the period of quiet Sun obtained by the SphinX detector. *I* — X-ray flux intensity

The solar radiation flux in the Lyman-α line measured on 28.02.2009 by the PHOKA radiometer was 5.7×10^{-3} W m^{-2} with an accuracy better than 15% [55]. This value is consistent with 5.77×10^{-3} W m^{-2} measured by SOLSTICE (SOLar STellar Irradiance Comparison Experiment) aboard the SORCE satellite on the same date.

During class-B and stronger flares, the contribution of the flaring vacuum UV radiation is at least 10% of the total solar disk luminosity in this range.

The SphinX (Solar photometer in X-rays), operating simultaneously with the TESIS telescope, is a high-sensitivity high-speed spectrophotometer to register soft X-ray solar radiation in the 0.85–15.00 keV energy band. The energy resolution is 0.1 keV and the time resolution is 1 s. SphinX is capable of registering variations of the solar soft X-ray emission with an amplitude 100 times smaller than radiometers aboard the GOES satellite. An example illustrating the potential of the detector is shown in Fig. 10, in which the variability of 5-min averaged soft X-ray flux detected in four months of observations is presented. The minimum values of the detected flux, which are 20 times smaller than the threshold of the GOES radiometer, apparently correspond to a fully quiet solar corona. The flux amplitude and its variability increase when active regions (whose numbers are shown in Fig. 10) are present on the solar disk. The detected increase by more than 10 times corresponds to the minimum level of solar coronal activity in the absence of flares in their common sense.

Most observational data on soft X-ray and hard radiation was obtained by the mission instruments for the two flares of 5 July 2009 (class C2.7) and 26 October 2009 (class C1.3).

The flare of 5 July 2009 started, according to GOES, at 07:07:00 UTC (Coordinated Universal Time) in the region of the disk with coordinates S26W01. At this time, the solar radiation hit the instruments after passing the upper atmospheric layers at the minimum altitude (the occultation altitude) 170 km. The change in the occultation altitude with time is shown in Fig. 11. The flux of vacuum UV radiation reached the satellite with attenuation, which is illustrated by the signal decrease from the PHOKA photometer (Fig. 11d). At 07:10:00 UTC, the flare luminosity started rapidly increasing in soft X-ray channels from several keV to 10 keV (Fig. 12). The flux in these channels attained a maximum in five minutes (temperature 1.27 keV, emission measure 2.4×10^{48} cm^{-3}). Then a rapid cooling phase

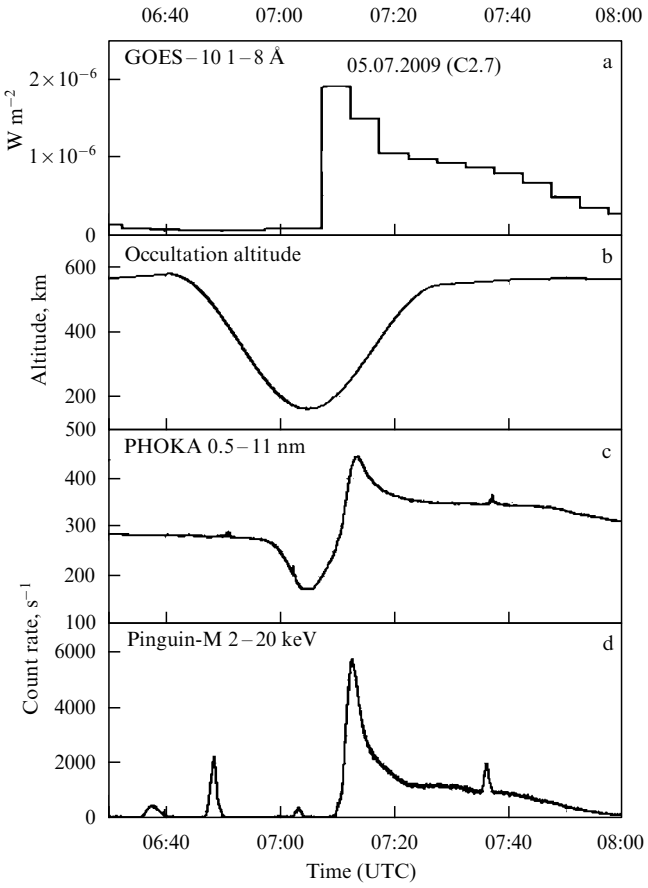

Figure 11. Soft X-ray light curve of the 5 July 2009 solar flare (class C2.7) registered by the GOES satellite and PHOKA and Pinguin-M detectors aboard CORONAS-PHOTON. The occultation dependence (b) suggests that the flare began at the instant of partial occultation of the satellite by the residual atmosphere of Earth.

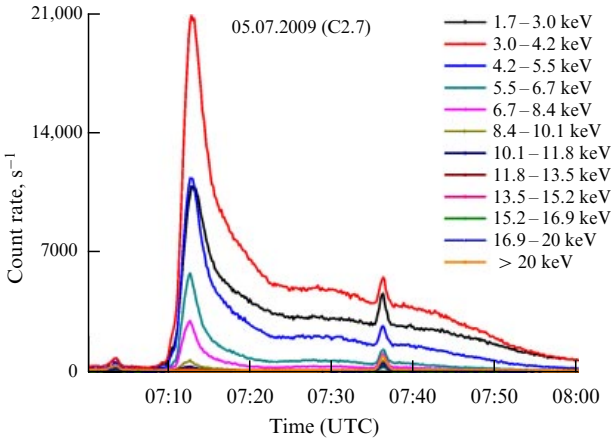

Figure 12. Soft X-ray intensity time profiles in the 5 July 2009 solar flare (class C2.7), which allow determining the dynamics of temperature and emission measure of the emitting region (data from the Pinguin-M detector).

occurred with the characteristic time scale of the flux decrease equal to 10 min by an order of magnitude, and then the cooling lasted for almost two hours. The behavior of harder radiation registered by the Konus-RF and RT-2 instruments is presented in Fig. 13. The acceleration of fast electrons started simultaneously with the warm phase and

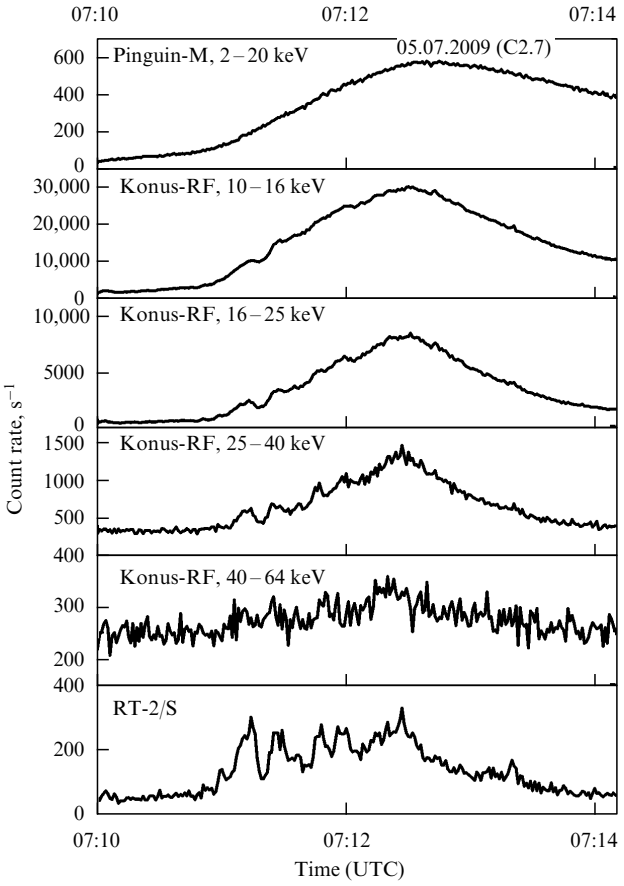

Figure 13. X-ray emission light curve of the 5 July 2009 solar flare registered in hard X-ray channels by Konus-RF and RT-2/S detectors.

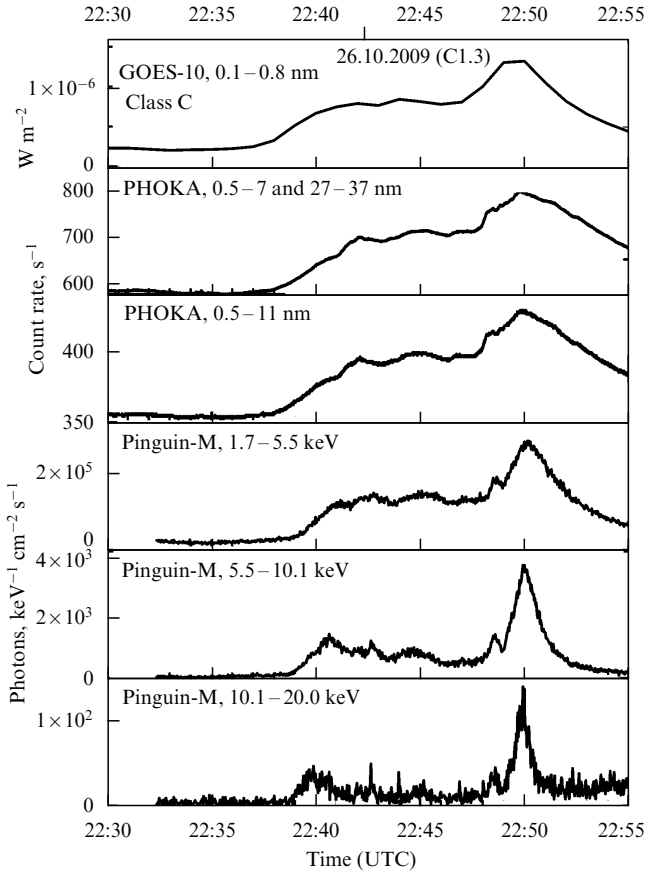

Figure 14. Soft X-ray light curve of the 26 October 2009 solar flare (class C1.3) registered by the GOES satellite and PHOKA and Pinguin-M detectors onboard CORONAS-PHOTON.

lasted (with almost equal rise and decay times) about three minutes. The maximum energy of photons registered by the Konus-RF instrument was at least 60 keV.

It is clearly seen that the time structure becomes more pronounced at high energies and is most distinct in the data obtained by the RT-2 detector, which has a lower background in hard X-rays due to the use of a phoswhich detector and a passive collimator. The analysis reveals the presence of QPOs with the periods 12 and 16 s [56]. Because a fairly slow propagating coronal ejection was observed simultaneously with this event, it is possible that the process of gradual formation of the plasmoid in the reconnection region explains oscillations with the observed periods.

The flare of 26 October 2009 started, according to GOES, at 22:38 UTC in the disk region with coordinates N19W35. The evolution of this flare in the vacuum UV range (channels of the PHOKA detector and soft X-ray channels of the Pinguin-M detector) is shown in Fig. 14. It is clearly seen that the evolution of both soft and X-ray fluxes from this flare is principally different from the previous one. Only soft thermal X-ray emission of a low variable intensity is initially observed. The characteristic time of variability (heating and cooling) is about 2 min. At 22 h 49 m UTC, the second phase started. It is characterized by the growth of hard X-ray emission with photon energies up to about 200 keV. Fluxes in hard X-ray channels from this flare recorded by the Konus-RF detector are shown in Fig. 15 in comparison with those from the previous flare. The comparison of these data shows that high-energy emission is present only in the weaker class flare, while the keV-channel intensity at a maximum in the C2.7 flare is higher by an order of magnitude.

The presence of hard radiation in the flare of 26 October 2009 allowed making polarization measurements by the Pinguin-M polarimeter with the aim to search for scattering anisotropy due to linear polarization of hard X-ray emission. With the account for the background from charged particles measured by the Electron-M-Peska detector aboard the satellite, the time interval from 22:49:31 UTC to 22:50:17 UTC was chosen for the analysis. The analysis carried out at MEPhI with the participation of the author led to the preliminary conclusion that the degree of polarization at that time was $(24 \pm 5)\%$. The importance of polarization measurements and several existing results were discussed above; here, we only mention that the spectrum-averaged effective area of the Pinguin-M polarimeter is 5 cm^2 (for comparison, the corresponding area of the SPR-N detector aboard the CORONAS-F satellite was 0.3 cm^2 at 20 keV and 1.5 cm^2 at 100 keV). In addition, instead of a traditional beryllium diffuser, four organic scintillators were used in the Pinguin-M detector. Signals from these scintillators switched on upon coincidence with those from detectors of the diffused radiation (absorbers), which drastically reduced the background contribution. The characteristics of all detectors were automatically stabilized and regularly calibrated by a built-in source.

We finally note an interesting result related to the X-ray albedo of the terrestrial atmosphere. Two identical Konus-RF detectors with the field of view up to 180° were installed

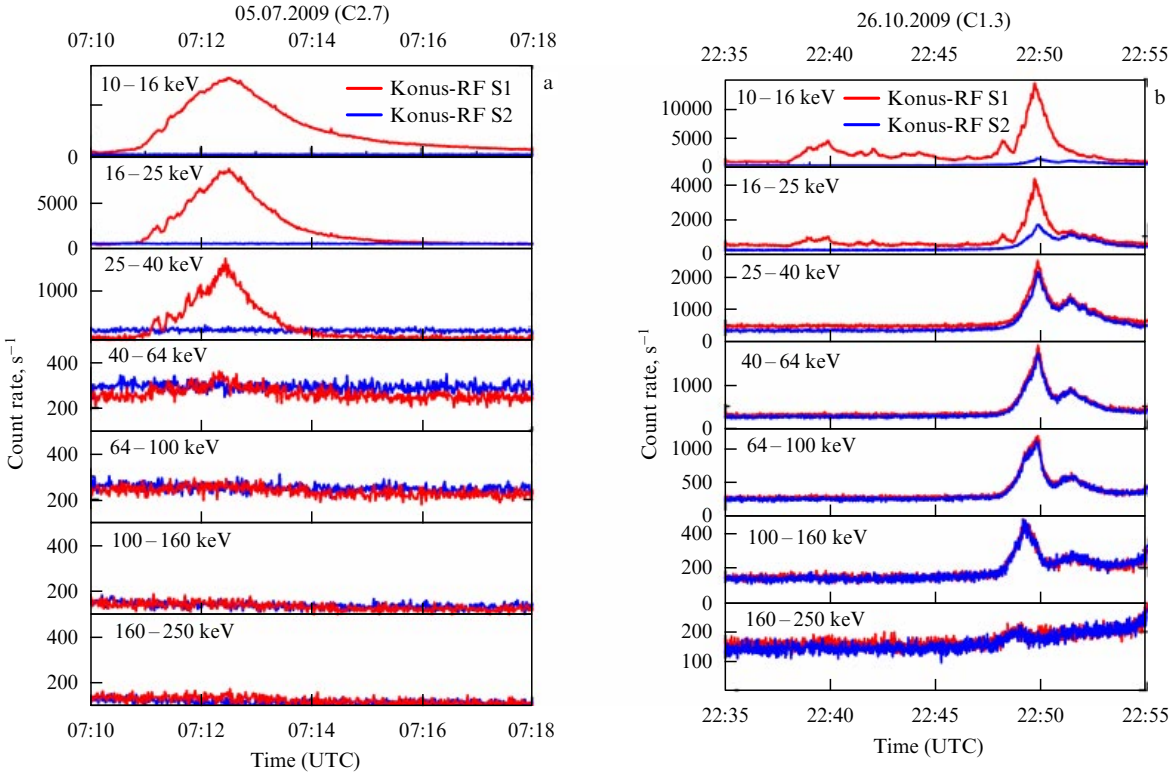

Figure 15. Comparison of the time dependence of the radiation intensity from two solar flares of 5 July 2009 (a) and 26 October 2009 (b), registered by the solar (S1) and anti-solar (S2) detectors of the Konus-RF instrument.

aboard the satellite in order to increase the operational time of searching for gamma-ray bursts, which are isotropically distributed in the sky. The axis of one of the detectors was directed toward the Sun, and the axis of the other was directed away from the Sun. Figure 15 shows the count rates of both detectors during the two solar flares discussed above. Apparently, the emission registered during the solar flare of 26 October 2009 by the anti-solar detector is the reflected flux from Earth's atmosphere. The increase in albedo with energy is connected with the absorption ratio and scattering cross sections in the atmosphere as a function of the photon energy. In particular, the value of the terrestrial X-ray albedo for space X-ray emission in the 1–1000 keV energy range calculated in [57] suggests that the maximum of the reflection coefficient falls within the range 30–100 keV, which is qualitatively consistent with our measurements.

This effect was not observed during the 5 July 2009 flare, which is due to the orientation of the satellite at the instant of the flare. As noted above, this flare coincided with the time of the satellite coming out of the partial occultation region, which in turn means that the satellite was oriented almost parallel to the atmosphere. The formation conditions of the X-ray albedo and the orientation of the anti-solar detector excluded detection of the flare radiation reflected by the atmosphere.

5. Conclusion

The calibration and tests carried out during the commissioning phase of operation of the CORONAS-PHOTON satellite from February to November 2009, and express analysis and processing of the data obtained, which are partially presented in this report, confirmed the generally nominal and smooth operation of all the scientific payload of the satellite. The data on several solar flares that occurred during this period confirmed the success of complex studies of solar activity with instruments of one satellite.

The design, manufacturing, launching, and exploitation of the CORONAS-PHOTON mission were carried out according to the Federal Space Program of Russia.

The participants in the CORONAS-PHOTON project acknowledge many specialists from federal and state bodies and research and industrial organizations of Russia and Ukraine for the work carried out at different stages of the project, from the design of scientific instruments and systems of the satellite before the launch to its launching and support of its operation in orbit until December 2009.

References

1. Aschwanden M J *Physics of Solar Corona* (Berlin: Springer-Verlag, 2004)
2. Zaitsev V V, Stepanov A V *Usp. Fiz. Nauk* **178** 1165 (2008) [*Phys. Usp.* **51** 1123 (2008)]
3. Priest E, Forbes T *Magnetic Reconnection: MHD Theory and Applications* (Cambridge: Cambridge Univ. Press, 2000) [Translated into Russian (Moscow: Fizmatliz, 2005)]
4. Aschwanden M J *Space Sci. Rev.* **101** 1 (2002)
5. Kuznetsov V D, in *Solnechno-zemnaya Fizika. Rezul'taty Eksperimentov na Sputnike KORONAS-F* (Solar-Terrestrial Physics. Results of the CORONAS-F Experiment) (Ed. V D Kuznetsov) (Moscow: Fizmatlit, 2009) p. 10
6. Zhitnik I A et al. *Astron. Vestn.* **39** 495 (2005) [*Solar Syst. Res.* **39** 442 (2005)]
7. Kotov Yu D et al., in *Solnechno-zemnaya Fizika. Rezul'taty Eksperimentov na Sputnike KORONAS-F* (Solar-Terrestrial Physics. Results of the CORONAS-F Experiment) (Ed. V D Kuznetsov) (Moscow: Fizmatlit, 2009) p. 178

8. Kuznetsov S N et al., in *Solnechno-zemnaya Fizika. Rezul'taty Eksperimentov na Sputnike KORONAS-F* (Solar-Terrestrial Physics. Results of the CORONAS-F Experiment) (Ed. V D Kuznetsov) (Moscow: Fizmatlit, 2009) p. 295
9. Dikpati M, de Toma G, Gilman P A *Geophys. Res. Lett.* **33** L05102 (2006)
10. Solar Cycle Prediction, http://solarscience.msfc.nasa.gov/predict.shtml
11. Veselovskii I S et al. *Kosmich. Issled.* **42** 453 (2004) [*Cosmic Res.* **42** 435 (2004)]
12. Panasyuk M I et al. *Kosmich. Issled.* **42** 509 (2004) [*Cosmic Res.* **42** 489 (2004)]
13. Grechnev V V et al. *Solar Phys.* **252** 149 (2008)
14. Chupp E L et al. *Astrophys. J.* **263** L95 (1982)
15. Forrest D J et al., in *Proc. of the 19th Intern. Cosmic Ray Conf., La Jolla, USA, 1985* Vol. 4, p. 3179
16. Kanbach G et al. *Astron. Astrophys. Suppl.* **97** 349 (1993)
17. Akimov V V et al. *Pis'ma Astron. Zh.* **18** 167 (1992) [*Astron. Lett.* **18** 69 (1992)]
18. Galper A M et al. *Pis'ma Zh. Eksp. Teor. Fiz.* **63** 889 (1996) [*JETP Lett.* **63** 931 (1996)]
19. Akimov V V et al. *Solar Phys.* **166** 107 (1996)
20. Talon R et al. *Solar Phys.* **147** 137 (1993)
21. Vilmer N et al. *Astron. Astrophys.* **412** 865 (2003)
22. Debrunner H, Lockwood J A, Ryan J M, in *Proc. of the 24th Intern. Cosmic Ray Conf., Rome, Italy, August 28 – September 8, 1995* Vol. 4 (Eds N Iucci, E Lamanna) (Roma: Intern. Union of Pure and Appl. Phys., 1995) p. 167
23. Djantemirov H M et al., in *Proc. of the 24th Intern. Cosmic Ray Conf., Rome, Italy, August 28 – September 8, 1995* Vol. 4 (Eds N Iucci, E Lamanna) (Roma: Intern. Union of Pure and Appl. Phys., 1995) p. 94
24. Tsuneta S *Astrophys. J.* **483** 507 (1997)
25. Aschwanden M J, in *Turbulence, Waves and Instabilities in the Solar Plasma* (Eds R Erdelyi et al.) (Dordrecht: Kluwer Acad. Publ., 2003)
26. Nakariakov V M, Melnikov V F *Space Sci. Rev.* **149** 119 (2009)
27. Jakimiec J, Tomczak M *Solar Phys.* **261** 233 (2010)
28. Terekhov O V et al. *Pis'ma Astron. Zh.* **28** 452 (2002) [*Astron. Lett.* **28** 397 (2002)]
29. Zaitsev A A, Stepanov A V *Pis'ma Astron. Zh.* **15** 154 (1989) [*Sov. Astron. Lett.* **15** 66 (1989)]
30. Stepanov A V, Urpo S, Zaitzev V V *Solar Phys.* **140** 139 (1992)
31. Nakariakov V M et al. *Astrophys. J.* **708** L47 (2010)
32. Lin R P et al., in *The Reuven Ramaty High-Energy Solar Spectroscopic Imager* (*RHESSI*) (Dordrecht: Kluwer Acad. Publ., 2002) p. 1
33. Chupp E L *Annu. Rev. Astron. Astrophys.* **22** 359 (1984)
34. Ramaty R, Murphy R J *Space Sci. Rev.* **45** 213 (1987)
35. Abramov V I, Kotov Yu D *Pis'ma Astron. Zh.* **13** 142 (1987) [*Sov. Astron. Lett.* **13** 58 (1987)]
36. Ramaty R, Mandzhavidze N *AIP Conf. Proc.* **522** 401 (2000)
37. Bogovalov S V, Kotov Yu D, Ustinov P L *Pis'ma Astron. Zh.* **23** 300 (1997) [*Astron. Lett.* **23** 263 (1997)]
38. Bogovalov S V et al. *Astron. Zh.* **65** 147 (1988) [*Sov. Astron.* **32** 76 (1988)]
39. Korchak A A *Dokl. Akad. Nauk SSSR* **173** 291 (1967) [*Sov. Phys. Dokl.* **12** 192 (1967)]
40. Somov S V, Tindo I P *Kosmich. Issled.* **16** 683 (1978)
41. Leach J, Petrosian V *Astrophys. J.* **269** 715 (1983)
42. Bogovalov S V, Kelner S P, Kotov Yu D *Astron. Zh.* **64** 1280 (1987) [*Sov. Astron.* **31** 672 (1987)]
43. Tindo I P et al. *Solar Phys.* **14** 204 (1970)
44. Tindo I P, Shuryghin A I, Steffen W *Solar Phys.* **46** 219 (1976)
45. Zhitnik I A et al., in *Solnechno-zemnaya Fizika. Rezul'taty Eksperimentov na Sputnike KORONAS-F* (Solar-Terrestrial Physics. Results of the CORONAS-F Experiment) (Ed. V D Kuznetsov) (Moscow: Fizmatlit, 2009) p. 128
46. McConnell M L et al. *Solar Phys.* **210** 125 (2002)
47. Boggs S E, Coburn W, Kalemci E *Astrophys. J.* **638** 1129 (2006)
48. Kotov Yu D, Bogovalov S V, Endalova O V *Izv. Ross. Akad. Nauk Ser. Fiz.* **61** 1201 (1997) [*Bull. Russ. Acad. Sci. Phys.* **61** 938 (1997)]
49. Ramaty R, Lingenfelter, Kozlovsky, in *The Light Elements and Their Evolution*: *Proc. of the 198th Symp. of the Intern. Astronomical Union, Brazil, 1999* (Eds L da Silva, M Spite, J R de Medeiros) (Provo, UT: Astron. Soc. of the Pacific, 2000) p. 51
50. Makridenko L A, Kotov Yu D, Boyarchuk K A, Volkov S N, Salikhov R S (Eds) *Kosmicheskii Kompleks "KORONAS-FOTON". Spravochnye Materialy* (Space Complex CORONAS-PHOTON. Handbook) (Moscow: FGUP NPP VNIIEM, 2008)
51. Nazirov R R, Chulkov I V, Yurov V N (Eds) *Pervye Etapy Letnykh Ispytanii i Vypolnenie Programmy Nauchnykh Issledovanii po Proektu KORONAS-FOTON* (First Stages of Flight Tests and Results of the Scientific Studies of the CORONAS-PHOTON Project) (Moscow: IKI RAS, 2010)
52. Kotov Yu D et al., in *Nauchnaya Sessiya MIFI-2009* (Scientific Session of MEPhI-2009) Vol. 1 (Moscow: NIYaU MIFI, 2009) p. 100
53. Arkhangel'sky A I et al. *Trudy NPP VNIIEM. Voprosy Elektrotekh.* **111** (4) 9 (2009)
54. TESIS, http://www.tesis.lebedev.ru/
55. LISIRD, http:// lasp.colorado.edu/lisird/index.html
56. Rao A R et al. *Astrophys. J.* **714** 1142 (2010)
57. Churazov E et al. *Mon. Not. R. Astron. Soc.* **323** 93 (2001)

PACS numbers: 42.62.Be, 87.50.W-, **87.63. – d**
DOI: 10.3367/UFNe.0180.201006i.0661

Laser physics in medicine

I A Shcherbakov

The Prokhorov General Physics Institute (GPI), Russian Academy of Sciences (RAS), cooperates with various organizations in the area of laser medicine, these being several Academy institutions: Institute for Laser and Information Technologies (ILIT), RAS; Institute for Spectroscopy, RAS; Institute for Analytical Instrumentation, RAS; Lomonosov Moscow State University; leading Russian medical centers: Fedorov Federal State Institution Intersectoral Research and Technology Complex Eye Microsurgery, Rosmedtechnology; Gertsen Moscow Oncology Research Institute, Roszdrav; Russian Medical Academy of Postgraduate Education; Bakulev Center for Cardiovascular Surgery, Russian Academy of Medical Sciences; Central Clinical Hospital No. 1, Russian Railways; and a number of commercial enterprises: OptoSystems, Visionica, New Energy Technologies, Laser Technologies in Medicine, Cluster, and the Scientific and Technological Center of Fiber-Optical Information-Measuring Systems.

The unique properties of a laser, which has the capacity to ultimately concentrate energy in space, time, and the spectral range, make this device an indispensable instrument in many areas of human activity, in medicine in particular.

Figure 1 shows the wavelengths of lasers that have found use in medical practice to some extent. We can see that the spectral domain ranges from the ultraviolet to the middle infrared. The energy density range spans three orders of magnitude (from 1 J cm^{-2} to 10^3 J cm^{-2}), the power density range spans 18 orders of magnitude (from 10^{-3} W cm^{-2} to 10^{15} W cm^{-2}), and the temporal range spans 16 orders of

I A Shcherbakov Prokhorov General Physics Institute, Russian Academy of Sciences, Moscow, Russian Federation
E-mail: director@gpi.ru

Uspekhi Fizicheskikh Nauk **180** (6) 661 – 665 (2010)
DOI: 10.3367/UFNr.0180.201006i.0661
Translated by E N Ragozin; edited by A M Semikhatov